Article

The Transmembrane Domain Peptide of Vesicular Stomatitis Virus Promotes Both Intermediate and Pore Formation during PEG-Mediated Vesicle Fusion

Tanusree Sengupta,[1,2] Hirak Chakraborty,[1,2] and Barry R. Lentz[1,2,*]
[1]Department of Biochemistry and Biophysics and [2]Program in Molecular and Cellular Biophysics, University of North Carolina at Chapel Hill, North Carolina

ABSTRACT We propose mechanisms by which the transmembrane domain of vesicular stomatitis virus (VSV-TMD) promotes both initiation of fusion and formation of a fusion pore. Time courses of polyethyleneglycol (PEG)-mediated fusion of 25 nm small unilamellar vesicles composed of dioleoylphosphatidylcholine, dioleoylphosphatidylethanolamine (DOPE), bovine brain sphingomyelin, and cholesterol (35:30:15:20 molar ratio) were recorded at pH 7.4 at five different temperatures (from 17°C to 37°C) and compared with time courses obtained with the same vesicles containing the fusion-active TMD of the G protein of VSV. Multiple time courses were fitted globally to a one-intermediate ensemble kinetic model to estimate the rate constants for conversion of the aggregated state to an intermediate hemifused state (k_1, stalk, or I_1) that rapidly transits to an unstable intermediate (I_2 state) that converts to a final fusion pore state with a combined rate k_3. The probabilities of lipid mixing, contents mixing, and contents leakage in the three states were also obtained from this analysis. The activation thermodynamics for each step were consistent with previously published models of lipid rearrangements during intermediate and pore formation. The influences of VSV-TMD, hexadecane, and VSV-TMD + hexadecane on the kinetics, activation thermodynamics, and membrane structure support the hypothesis that these two agents do not catalyze fusion by a common mechanism, except possibly at the lowest temperatures examined. VSV-TMD primarily catalyzed initial intermediate formation, although it substantially increased the probability of contents mixing in the intermediate state. Our results support the hypothesis that the catalytic influence of VSV-TMD on the initial-intermediate- and pore-forming steps of PEG-mediated fusion derives from its ability to impose a positive intrinsic curvature and thereby stress small unilamellar vesicle outer leaflets as well as the periphery of intermediate microstructures.

INTRODUCTION

Biological membrane fusion is observed in many vital intra- and intercellular events, such as viral infection, neurotransmission, protein trafficking, and fertilization. Since membranes with mammalian membrane-like compositions do not generally fuse spontaneously, membrane fusion is mediated by protein machinery in living systems. The entry of enveloped viruses into cells requires the fusion of cellular and viral membranes triggered by conformational changes in viral glycoproteins. Based on their molecular architecture, viral fusion proteins fall into one of three classes. In class I fusion proteins (e.g., influenza hemagglutinin and paramyxovirus F protein) the post-fusion trimer displays a six-helix bundle with a fusion peptide at the N-terminus of the central helices and the transmembrane domains (TMDs) at the C-terminus of the antiparallel outer helices existing in the same common membrane postfusion (1,2). Class II fusion proteins are composed mainly of β sheets and their internal fusion peptides are embedded in the ectodomain (3). Class III is a comparatively newly identified group whose members include fusion proteins from rhabdoviruses, herpesviruses, vesicular stomatitis virus (VSV), and baculoviruses. Despite some diversity, all characterized viral fusion proteins convert from a fusion-competent state to a state that embeds the fusion peptide in the target membrane, whereas the TMD remains attached to the viral membrane. The free energy associated with a conformational change in the fusion protein is proposed to bring these two membranes into close proximity (4), a condition required for fusion (5).

Several reports have demonstrated the importance of the TMD region of viral fusion proteins in the fusion process. Replacement of the TMD of influenza hemagglutinin (6,7) and VSV G protein (8) by a glycerylphosphatidylinositol (GPI) anchor abolished fusion. Several studies showed that certain residues in TMD sequences of HIV (9–11) or VSV (12,13) are critical for fusion. All of these studies demonstrated the importance of viral fusion protein TMDs to fusion, but in general failed to address the detailed mechanisms by which these TMDs promote fusion. Although some reports pointed to a role of TMD in formation of

Submitted August 29, 2013, and accepted for publication March 6, 2014.

*Correspondence: uncbrl@med.unc.edu

Hirak Chakraborty and Tanusree Sengupta contributed equally to this work.

Hirak Chakraborty's present address is CSIR-Centre for Cellular & Molecular Biology, Hyderabad 500007, India.

Tanusree Sengupta's present address is Department of Biotechnology, Indian Institute of Technology Madras, Chennai 600036, India.

Editor: William Wimley.

0006-3495/14/09/1318/9 $2.00

http://dx.doi.org/10.1016/j.bpj.2014.03.053

hemifusion intermediates (6,7,14), others indicate a possible role later in the fusion process (12,13). Some have suggested that they might deform the lipids surrounding them, which would result in dimples and thus favor formation of a stalk (15,16), whereas others have suggested that they might occupy interstice space (a region of imperfect acyl-chain packing at the interface between lamellar and nonlamellar regions of fusing membranes (17) to stabilize fusion intermediates (13). Here, we present a detailed analysis of the kinetics of polyethyleneglycol (PEG)-triggered fusion of an ensemble of DOPC/DOPE/SM/CH (35:30:15:20) small unilamellar vesicles (SUVs) at pH 7.4 at five temperatures in the presence of VSV-TMD. The activation thermodynamics for fusion of these vesicles in the absence of VSV-TMD at pH 7.4 are reported in an accompanying paper (18) and are consistent with mechanistic models we proposed earlier for pH 5 (19) once the altered hydration of DOPE at pH 7.4 is taken into account.

VSV, a member of the Rhabdoviridae viruses, enters the cell via an endocytic pathway and subsequently fuses with a cellular membrane within the acidic environment of the endosome (20), where fusion is mediated by a single transmembrane viral glycoprotein (G) that is trimeric and forms the spikes that protrude from the viral surface (21). Earlier studies showed that mutation of two Gly to Ala (see sequence in Materials section) in the TMD of this G protein inhibited fusion in our model system (13) as it did in ex vivo studies (12). A crude analysis of the initial rates of lipid mixing (LM) and contents mixing (CM) tentatively suggested that VSV-TMD influenced mainly the final step of pore formation (CM) as opposed to the step of initial intermediate formation (LM) (13). However, both the initial and final steps of fusion involve both LM and CM (22,23), so such a simplified analysis cannot yield mechanistic detail. In this study, we measured LM, CM, and contents leakage (CL) at five different temperatures in the presence and absence of the VSV-TMD peptide, and fitted the data to our previously well-documented ensemble kinetic model of the fusion process (19,22). In this way, we determined the rate constants for the interconversion of states as well as the probability of observing CM, LM, or CL in each state, and revealed in detail the effects of VSV-TMD on each step of the fusion process. In addition, we report the activation thermodynamics for all steps and use this information to propose mechanisms by which the VSV-TMD peptide might catalyze each step. To aid in interpreting the effects of VSV-TMD on the activation thermodynamics, we also recorded the effects of VSV-TMD on the membrane bilayer properties, as well as the fusion kinetics in the presence of both VSV-TMD and 2 mol % hexadecane (a known interstice-occupying agent). Finally, we propose possible mechanisms by which VSV-TMD might catalyze fusion in our model system, and use our findings to test the previously proposed hypothesis that VSV-TMD might promote fusion by occupying interstice space (13).

MATERIALS AND METHODS

Materials

The VSV-TMD peptide with sequence (K)KSSIASFFFII**G**LII**G**LFLVLR(R) used in this study was synthesized by Invitrogen. Chloroform stock solutions of 1,2-dioleoyl-3-phosphatidylcholine (DOPC), 1,2-dioleoyl-3-sn-phosphatidylethanolamine (DOPE), and bovine brain sphingomyelin (SM) were purchased from Avanti Polar Lipids (Birmingham, AL) and used without further purification. The concentrations of all of the stock phospholipids were determined by a phosphate assay (24). Cholesterol (CH) was purchased from Avanti and then purified as described previously (25). We obtained 2-(4,4-difluoro-5,7-diphenyl-4-bora-3a,4a-diaza-s-indacene-3-dodecanoyl)-1-hexadecanoyl-*sn*-glycero-3-phosphoethanolamine (BODIPY530-PE) and 2-(4,4-difluoro-5,7-diphenyl-4-bora-3a,4a-diaza-s-indacene-3-dodecanoyl)-1-hexadecanoyl-*sn*-glycero-3-phosphocholine (BODIPY500-PC) from Molecular Probes (Eugene, OR). Terbium chloride and N-[tris(hydroxymethyl)methyl]2-2-aminoethane sulphonic acid (TES) were purchased from Sigma Chemical (St. Louis, MO). PEG of molecular weight 7000–9000 (PEG 8000) was purchased from Fisher Scientific (Fairlane, NJ) and further purified as previously described (26). Dodecyl octaethylene glycol monoether ($C_{12}E_8$) was purchased from Calbiochem (La Jolla, CA). All other reagents were of the highest purity grade available.

Methods

Most methods used in this study have been reported previously and are also described in an accompanying article (18). VSV-TMD peptide was dissolved in trifluoroethanol/water (95:5 vol/vol) mixture. We incorporated VSV-TMD into SUVs by adding it at a 1:600 peptide/lipid ratio to a chloroform mixture of phospholipids prior to freeze-drying and sonication. This is the highest mol fraction that could be used to recover intact SUVs. Because so little peptide could be incorporated, we were unable to reliably determine the orientation of the peptide in the bilayer without a very expensive custom synthesis of fluorescently tagged peptides. Because the packing constraints of SUVs are considerable and force other TMD peptides we have studied to insert roughly asymmetrically, we assume this is the case for VSV-TMD as well.

Fusion model

We analyze our data in terms of a sequential, multistep model that was previously described in detail (19,22). In our experiments, SUVs are brought rapidly into close contact (the aggregation rate is 10-fold higher than the rate of any fusion event) by addition of PEG to form an aggregated state (referred to as the A state in our model). This avoids the complication of vesicle diffusion in our data analysis. The A state converts to a fusion intermediate (I) state at a rate k_1. This involves a change in system topology, since contacting or *cis* bilayer leaflets merge during this step (hemifusion; see Fig. S3 in the Supporting Material). Finally, the I state converts slowly (rate k_3) to a final fusion pore (FP) state, an event that also occasions a change in system topology. Experimentally, we track the process by monitoring LM between vesicle membranes, CM between vesicle compartments, and CL from the vesicle compartments, all of which can occur in the A, I, or FP state with probabilities α_i (CM), β_i (LM), and λ_i (CL), where i is 0 for the A state, 1 for the I state, and 3 for the FP state. Because of the normalization conditions used and experimental observations, a total of seven parameters (two k_i, α, and β, and three λ_i) are required to describe three double-exponential curves, which guarantees that the model will not be underdetermined as long as all three data sets are analyzed globally. The probabilistic quantities α and β, as well as the leakage rates λ_i, are required because our kinetic model describes the passage of an ensemble of vesicles through thermodynamic states leading to fusion. Individual fusing vesicle pairs or aggregates are not identical structurally, and they do not travel through phase space in concert. In our ensemble measurements, we average over many events that occur between vesicles brought rapidly into close contact

by addition of PEG. To obtain kinetics from single-event studies, one must record many traces of events that follow initiation of fusion between docked membranes (vesicles attached to other vesicles or to membranes) and then analyze the time probability distributions (dwell-time distributions) to distinguish distinct events and obtain their characteristic times (rates). Elsewhere (27), we describe in detail the relationship between the ensemble approach and a well-documented single-event study of fusion of docked vesicles (28), and show that pictures of fusion obtained by the two methods are consistent. Although both approaches have advantages and disadvantages, ensemble measurements have the advantage of requiring much shorter experiment times. This allowed us to examine the influence of many variables (e.g., pH (18) and fusion peptides (27)) on the kinetics and activation thermodynamics for each step of the fusion process by performing experiments at five different temperatures (17°C, 22°C, 27°C, 32°C, and 37°C). It also allowed us to collect precise data, in that all experiments were repeated twice for any given sample and then repeated for three different sample preparations at a given temperature. The kinetic parameter values are the averages of all these determinations. In an accompanying article (18), we document the kinetics and activation thermodynamics of PEG-mediated fusion of the DOPC/DOPE/SM/CH (35:30:15:20) SUVs used in our experiments at pH 7.4. In addition, we explore the role of pH in determining the mechanism of each step of the fusion process, as well as the influence of hexadecane on each step. Detailed descriptions of the ensemble kinetic model, the kinetic parameters for the control vesicles, and the equations used to obtain the activation thermodynamics are also given in that work.

RESULTS

Effect of VSV-TMD on PEG-mediated fusion

Fig. 1 shows in red the time courses of LM, CM, and CL for SUVs containing VSV-TMD at a peptide/lipid ratio of 1:600 at 22°C and pH 7.4 as compared with data obtained with control vesicles (*green*) (18). Data obtained at each temperature were analyzed globally according to a single-intermediate model. Kinetic parameters obtained at 22°C and 37°C are summarized in Table 1 and parameters obtained at other temperatures are presented in Table S1. When compared with results obtained with control vesicles lacking VSV-TMD (18), the results show that VSV-TMD had no substantial effect on the extent of LM (F_{LM}) or CM (F_{CM}) or on the probability of LM in the intermediate state (β). It had the greatest effects on the rate of initial intermediate formation (k_1), the rate of leakage from unfused vesicles (λ_0), and the probability of CM in the intermediate state (α). VSV-TMD also increased k_3 slightly at low (but not high) temperatures and had moderate effects on leakage rates λ_1 and λ_3. To understand the role of VSV-TMD in promoting the rate of I formation and the extent of pore formation, we examined the activation thermodynamics of I formation and the nature of pore formation from I.

Effect of VSV-TMD on the activation thermodynamics of PEG-mediated fusion

We similarly determined the temperature dependence of the activation free energy for formation of the I_1 state and FP state in the presence of VSV-TMD at pH 7.4 and compared

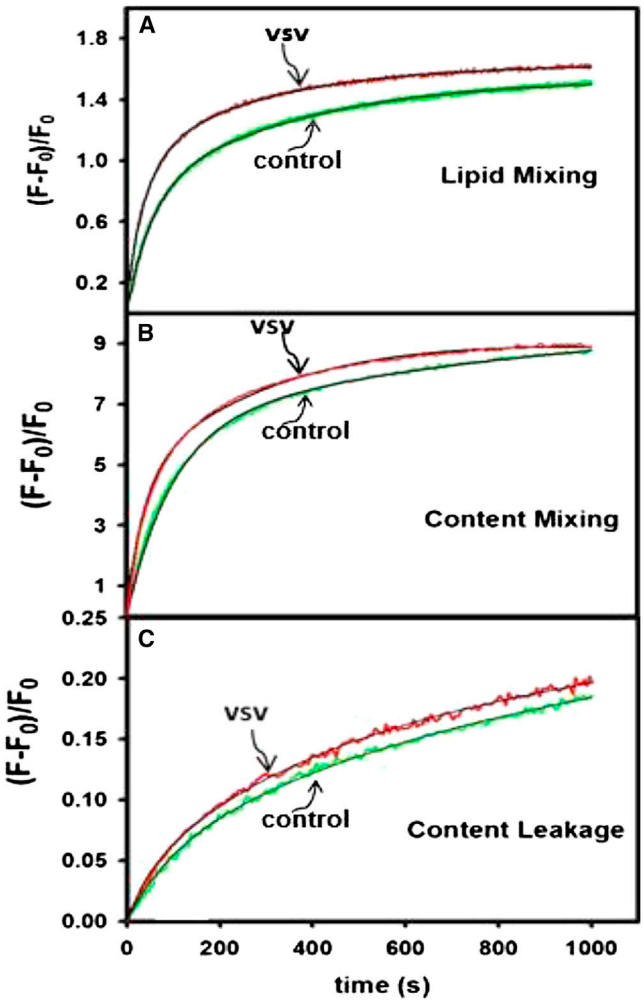

FIGURE 1 Effect of VSV-TMD peptides on the kinetics of (*A*) LM, (*B*) CM, and (*C*) CL during 5 wt % PEG-mediated SUV fusion at 22°C. Time courses are shown for peptide-free vesicles (*green*) as well as vesicles containing VSV-TMD (*red*) at a P/L ratio of 1:600. The black lines are the best fit of the data obtained using the one-intermediate model (18). To see this figure in color, go online.

the results with the activation thermodynamics of control DOPC/DOPE/SM/CH (35:30:15:20) (18). Fig. 2, *A* and *C*, show the change in activation free energy associated with the presence of VSV-TMD in vesicle membranes ($\Delta\Delta G_i^* = \Delta G_{i,peptide}^* - \Delta G_{i,control}^*$) for formation of the I state and FP state, respectively. The changes in activation enthalpy ($\Delta\Delta H_i^*$) and activation entropy ($T\Delta\Delta S_i^*$), as plotted in Fig. 2, *B* and *D*, for formation of the I state and FP state, respectively, were obtained as derivatives of $\Delta\Delta G_i^*$ as described elsewhere (18,19). The signs of $\Delta\Delta H_i^*$ and relative magnitudes of $T\Delta\Delta S_i^*$ define whether the catalytic effect was entropic ($T\Delta\Delta S_i^* > \Delta\Delta H_i^* > 0$) or enthalpic ($\Delta\Delta H_i^* < T\Delta\Delta S_i^* < 0$). The insets in Fig. 2, *B* and *D*, show the changes in activation heat capacity ($\Delta\Delta Cp_i^*$) associated with the presence of VSV-TMD. The temperature dependence of $\Delta\Delta Cp_i^*$ reflects the nonlinear dependence of

TABLE 1 Kinetic constants for PEG-mediated fusion of PC/PE/SM/CH (35:30:15:20) SUVs containing or not containing VSV-TMD, and in the presence or absence of 2% hexadecane at low and high temperatures

	$k_1 \times 10^3$ (s^{-1})	$k_3 \times 10^3$ (s^{-1})	α	β	$\lambda_0 \times 10^4$	$\lambda_1 \times 10^4$	$\lambda_3 \times 10^4$	f_{CM}	$(1-\alpha) \times f_{CM}$	f_{LM}
22°C_con	16.0 ± 0.5	1.69 ± 0.01	0.18 ± 0.010	0.66 ± 0.012	2.28 ± 0.07	2.09 ± 0.1	0.49 ± 0.17	0.25 ± 0.01	0.21 ± 0.004	0.43 ± 0.02
22°C_VSV	26.3 ± 0.28 64%	2.48 ± 0.03 47%	0.44 ± 0.021	0.63 ± 0.015	7.87 ± 0.21	3.8 ± 0.1	0.72 ± 0.16	0.26 ± 0.01	0.15 ± 0.01	0.45 ± 0.01
22°C_hex	17.0 ± 0.35 6.25%	2.21 ± 0.03 31%	0.57 ± 0.025	0.64 ± 0.022	7.73 ± 0.06	3.49 ± 0.05	0.32 ± 0.02	0.37 ± 0.01	0.16 ± 0.02	0.44 ± 0.02
22°C_hex + VSV	26.0 ± 0.46 ***0%***	2.79 ± 0.04 ***12%***	0.60 ± 0.01	0.64 ± 0.01	18.3 ± 0.02	4.8 ± 0.1	0.5 ± 0.2	0.36 ± 0.02	0.14 ± 0.02	0.43 ± 0.02
37°C_con	66.8 ± 1.5	3.03 ± 0.04	0.36 ± 0.021	0.72 ± 0.03	40.28 ± 0.35	7.24 ± 0.07	8.99 ± 0.28	0.33 ± 0.01	0.21 ± 0.01	0.46 ± 0.02
37°C_VSV	117.9 ± 2.0 76%	3.36 ± 0.03 11%	0.56 ± 0.011	0.77 ± 0.04	51.9 ± 0.5	8.62 ± 0.07	11.50 ± 0.38	0.34 ± 0.02	0.15 ± 0.02	0.47 ± 0.03
37°C_hex	89.0 ± 2.3 33%	3.83 ± 0.15 26%	0.68 ± 0.023	0.75 ± 0.03	87.87 ± 0.31	7.87 ± 0.36	4.96 ± 0.45	0.43 ± 0.03	0.14 ± 0.01	0.46 ± 0.02
37°C_hex + VSV	95.9 ± 1.6 ***18.7%***	3.64 ± 0.11 ***0%***	0.66 ± 0.02	0.74 ± 0.03	83.9 ± 0.2	9.1 ± 0.2	8.6 ± 0.5	0.42 ± 0.01	0.14 ± 0.02	0.47 ± 0.03

The percentages beside the k_1 and k_3 values for VSV-TMD and hexadecane alone are changes relative to control, and the percentages below VSV-TMD + hexadecane (shown in bold italics) are relative to control + VSV-TMD.

$\Delta\Delta H_i^*$ and $T\Delta\Delta S_i^*$ on temperature. There are substantial similarities but also differences between the changes in activation thermodynamics due to VSV-TMD associated with the first and second steps. Among the similarities, $\Delta\Delta Cp_1^*$ and $\Delta\Delta Cp_3^*$ both switch from positive to negative with increasing temperature. The most noticeable difference is that VSV-TMD catalyzes step 1 entropically (i.e., $T\Delta\Delta S_1^* > \Delta\Delta H_1^* > 0$) over the entire temperature range, whereas it catalyzes step 3 enthalpically (i.e., $\Delta\Delta H_3^* < T\Delta\Delta S_3^* < 0$). This difference indicates that VSV-TMD catalyzes steps 1 and 3 by different mechanisms, as discussed below.

Combined catalytic influence of hexadecane and VSV-TMD

Fig. 3 illustrates how VSV-TMD and hexadecane influence fusion individually and in each other's presence. One can see the very minimal catalytic influence of hexadecane on step 1 at low temperatures (18) in Fig. 3 *A* by comparing ΔG_1^* for control (●) versus hexadecane-containing vesicles (▼). VSV-TMD catalyzes step 1 over the entire temperature range (○). Of particular note is the fact that hexadecane interferes with the catalytic effect of VSV-TMD at the highest two temperatures examined (△), where hexadecane itself has a catalytic effect. As shown in Fig. 3 *C* and elsewhere (18), both hexadecane and VSV-TMD catalyze step 3 over the entire temperature range, but hexadecane enhances the catalytic influence of VSV-TMD only at the two lowest temperatures examined (Fig. 3 *B*). At the highest temperature, hexadecane has a greater catalytic influence than VSV-TMD, and the effect of both together is indistinguishable from that of hexadecane alone (Fig. 3 *B*). Clearly, the effect of hexadecane on the catalytic influence of VSV-TMD varies substantially with temperature for both steps 1 and 3, with the mechanism of hexadecane's influence differing from that of VSV-TMD at high temperatures, but perhaps being similar at low temperatures.

Effect of VSV-TMD and hexadecane on bilayer properties

We examined the influence of VSV-TMD on the bilayer properties of SUVs in the absence and presence of 2 mol % hexadecane. We explored the bilayer properties using three different fluorescent probes that report on different regions and properties of the membrane: C_6NBDPC, DPH, and TMA-DPH. Because C_6NBDPC partitions between its own micelles and membranes, its fluorescence lifetime components reveal the partition coefficient between these two phases, with the mol fraction of C_6NBDPC in the membrane providing a partition coefficient that is sensitive to the free volume within membrane outer leaflets (29). The τ_{D_2O}/τ_{H_2O} ratio of TMA-DPH is not altered by the presence of either VSV-TMD or hexadecane at any temperature

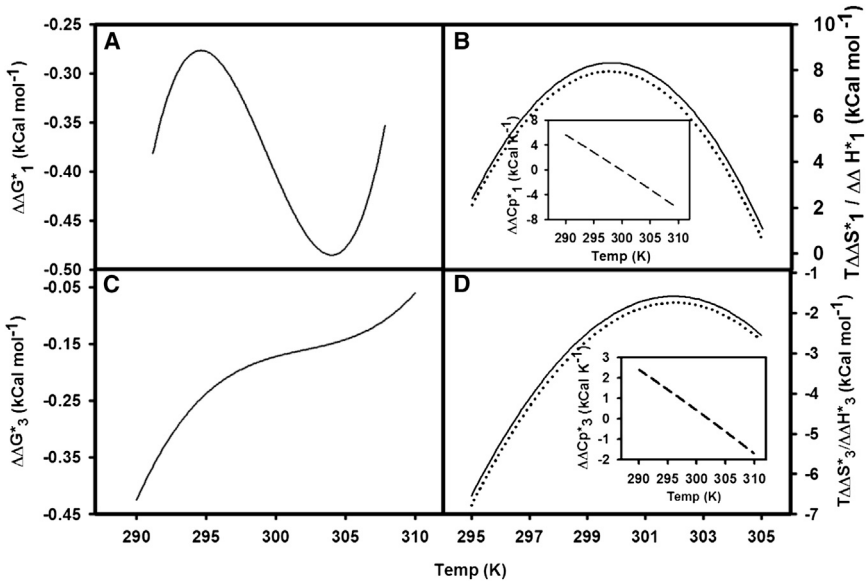

FIGURE 2 Temperature dependence of changes in activation free energy ($\Delta\Delta G_i^*$), activation entropy ($T\Delta\Delta S_i^*$), and activation enthalpy ($\Delta\Delta H_i^*$) of control vesicles induced by the presence of VSV-TMD peptide. (*A* and *C*) Activation free energy ($\Delta\Delta G_i^*$) versus temperature for steps 1 and 3, respectively. (*B*) $T\Delta\Delta S_1^*$ (*solid line*) and $\Delta\Delta H_1^*$ (*dotted line*) for intermediate formation. (*D*) $T\Delta\Delta S_3^*$ (*solid line*) and $\Delta\Delta H_3^*$ (*dotted line*) for pore formation. Insets show the temperature dependence of changes in activation heat capacity ($\Delta\Delta Cp_i^*$) in the presence of the peptide for each step. Coefficients of the polynomials obtained from the raw plots of ΔG^* versus T for the vesicles containing TMD are given in Table S2. The plots in *B* and *D* were obtained from those in *A* and *C* by differentiation.

(Fig. S1), so exposure of its amine group to water remains unaltered by these two perturbants. Except at the lowest temperature examined (17°C), neither VSV-TMD nor hexadecane ordered the bilayer interior, and even at this temperature the ordering effects were barely significant (Fig. S2). The lifetime of C_6NBDPC is sensitive to the polarity of its environment, which one can alter either by altering the extent of water penetration to the probe or by relocating the probe. Normally, C_6NBDPC is located just below the interface region of the bilayer (30), but bilayer perturbation can cause it to penetrate deeper (29). The temperature dependencies of the mol fraction and fluorescence lifetime of C_6NBDPC in control SUVS (●) and in membranes containing VSV-TMD (○) or hexadecane (▼), or both VSV-TMD and hexadecane (△) are presented in Fig. 4, *A* and *B*, respectively. VSV-TMD occupied the bilayer free volume at all temperatures, but its space-filling ability was greatest at the three lowest temperatures and decreased with temperature (Fig. 4 *A*). It reduced surface packing at all temperatures (Fig. 4 *C*) and promoted water penetration into the headgroup region (Fig. 4 *D*). Consistent with these effects, the NBD moiety of C_6NBDPC was in a less polar environment in the presence of VSV-TMD (i.e., either protected from water or penetrating deeper into the bilayer; Fig. 4 *B*). In summary, VSV-TMD seems to occupy the bilayer space in such a way that it spreads headgroups, which increases positive curvature stress. This could reflect a tilt of the VSV-TMD helix relative to the bilayer normal or simply a mismatch of protein structure with lipid packing. Since the native VSV-TMD appears to be a helix bent at the helix-breaking GXXXG sequence (13), and the peptide we used has sufficient nonpolar residues (20) to span the bilayer, the latter explanation is most likely.

Hexadecane produced no change in the polarity of the NBD environment (Fig. 4 *B*), but did reduce the bilayer free volume at all but the lowest temperature, and its ability to do so increased and then decreased with increasing temperature (Fig. 4 *A*). It did not influence interfacial order and water penetration at low temperatures, but increased interfacial order (Fig. 4 *C*) and decreased water penetration into the interface with increasing temperature (Fig. 4 *D*). The temperature dependence of hexadecane's structural influence (Fig. 4) suggests different hexadecane conformational ensembles at low and high temperatures, i.e., aligned with acyl chains and having little influence on membrane structure at low temperature, but having an increasingly broad conformational ensemble with increasing temperature. At the highest temperatures examined, this conformational ensemble appears to increase the acyl-chain cross section deep in the bilayer sufficiently to decrease water penetration of the interface (Fig. 4 *D*) and order the interface (Fig. 4 *C*), i.e., to produce an intrinsic negative curvature.

Of greatest interest was the combined effect of hexadecane and VSV-TMD. At the lowest temperature (290 K), hexadecane did not significantly reduce the bilayer free volume in the presence or absence of VSV-TMD (Fig. 4 *A*). With increasing temperature, the volume-reducing effects of hexadecane and VSV-TMD became increasingly additive. Given what we have observed regarding their individual influences, this is not surprising, since they should alter packing in different parts of the bilayer at these temperatures (with hexadecane occupying space deep in the bilayer and VSV-TMD doing so in the upper regions). This is especially evident in the temperature dependence of TMA-DPH anisotropy (Fig. 4 *C*) and lifetime (Fig. 4 *D*), where the surface-expanding influence of VSV-TMD and the surface-contracting effect of hexadecane completely nullify each other at high temperature. Whereas hexadecane had no effect on the polarity experienced by the NBD probe, hexadecane enhanced the probe-shielding effect of VSV-TMD

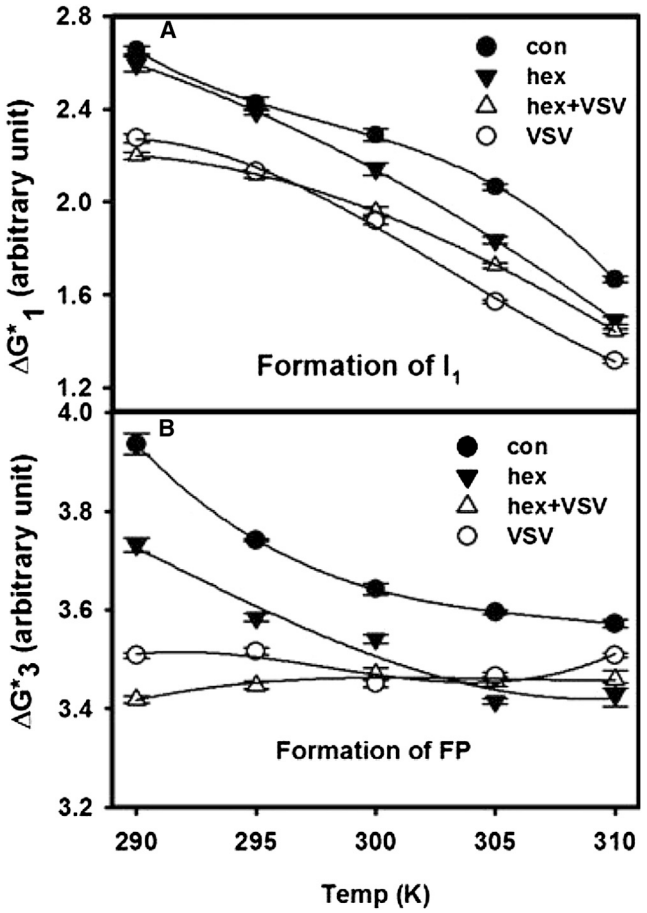

FIGURE 3 (*A* and *B*) Temperature dependence of the free-energy barrier for formation of (*A*) I_1 state (ΔG_1^*) and (*B*) pore formation (ΔG_3^*) for control vesicles (●), vesicles in the presence of VSV-TMD (○), vesicles containing 2 mol % hexadecane (▼), and vesicles containing 2 mol % hexadecane in the presence of VSV-TMD (△).

(Fig. 4 *B*). This is consistent with VSV-TMD disrupting interfacial packing but also filling the bilayer space and promoting penetration of the NBD probe to deeper regions of the bilayer, where hexadecane would fill the hydrophobic space and reduce polarity.

To summarize, the individual and combined effects of VSV-TMD and hexadecane support the hypothesis that hexadecane aligns with acyl chains at low temperatures and has little influence on bilayer structure except to occupy space, whereas it appears to alter membrane structure with increasing temperatures and disproportionately occupies the interior hydrophobic space. VSV-TMD, on the other hand, has the same membrane-altering influence at all temperatures, namely, filling space but disrupting interfacial packing and promoting water penetration into the interface. These observations highlight the different space-filling abilities of a flexible agent such as hexadecane, which is free to locate in different regions of the bilayer, as opposed to the more rigid VSV-TMD, which adopts a bent but roughly helical (~50%) conformation in a membrane (13).

DISCUSSION

We have found that a sequential, two-intermediate model for fusion is able to account for the ensemble kinetics of the fusion process for a variety of membrane systems (19,22,31,32) over a range of temperatures (19). Our ensemble kinetic treatment is based on the expanded stalk structural model for fusion (33) as modified to treat the highly curved, space-encapsulating membranes of SUVs (17). The model is illustrated in Fig. S3. Based on earlier observations (19,27), formation of an initial fusion intermediate (I_1 in Fig. S3) was proposed to occur through an unstable transition state (TS1) in which acyl chains are somewhat exposed to the dehydrated interbilayer space, thereby disrupting water-water and water-headgroup interactions in that space. Coarse-grained (34) and all-atom (35) MD simulations support this proposal. These observations also support the hypothesis that the final step of the fusion process (FP formation) involves passage through another unstable transition state (TS3), which is distinguished from the I_2 semistable intermediate (Fig. S3) only by the probability of coordinated multilipid fluctuations in which lipids from both the *cis* and *trans* leaflets of the I_2 intermediate cooperatively enter the highly unfavorable interstice region (17) of this semistable intermediate (19,27). In this work, we ask whether the effects of VSV-TMD on the kinetics and activation thermodynamics of the fusion process at pH 7.4, as well as on the measured bilayer structure, can be interpreted in terms of these mechanistic pictures of the individual steps of the fusion process.

Step 1: initial intermediate formation

The catalytic effect of VSV-TMD on step 1 was substantial, with k_1 being increased by 64% at 22°C and by 76% at 37°C (Tables 1 and S1). Catalysis by VSV-TMD was entropic ($T\Delta\Delta S_1^*>\Delta\Delta H_1^*>0$) over the entire temperature range (Fig. 2 *B*), implying that the presence of VSV-TMD either increased the number of energetically closely spaced microstructures in the transition state (TS1) leading to the stalk intermediate or stabilized a few microstructures in state A. The positive $\Delta\Delta Cp_1^*$ at low temperature is consistent with increased water ordering in TS1 due to increased acyl-chain migration into the interbilayer space. The fact that $\Delta\Delta Cp_1^*$ became increasingly negative with increasing temperature (Fig. 2 *B*, *inset*) is consistent with the expected reduction of water ordering by hydrocarbon with increasing temperature and with hexadecane decreasing the width of the energy distribution in TS1. According to our membrane structural measurements (Fig. 4, *C* and *D*), VSV-TMD does not appear to accommodate well to the packing of acyl chains and thus disorders and permits water entry into the interface, thereby increasing positive curvature stress in contacting outer leaflets of SUVs at all temperatures. This should encourage escape of acyl chains into the interbilayer space,

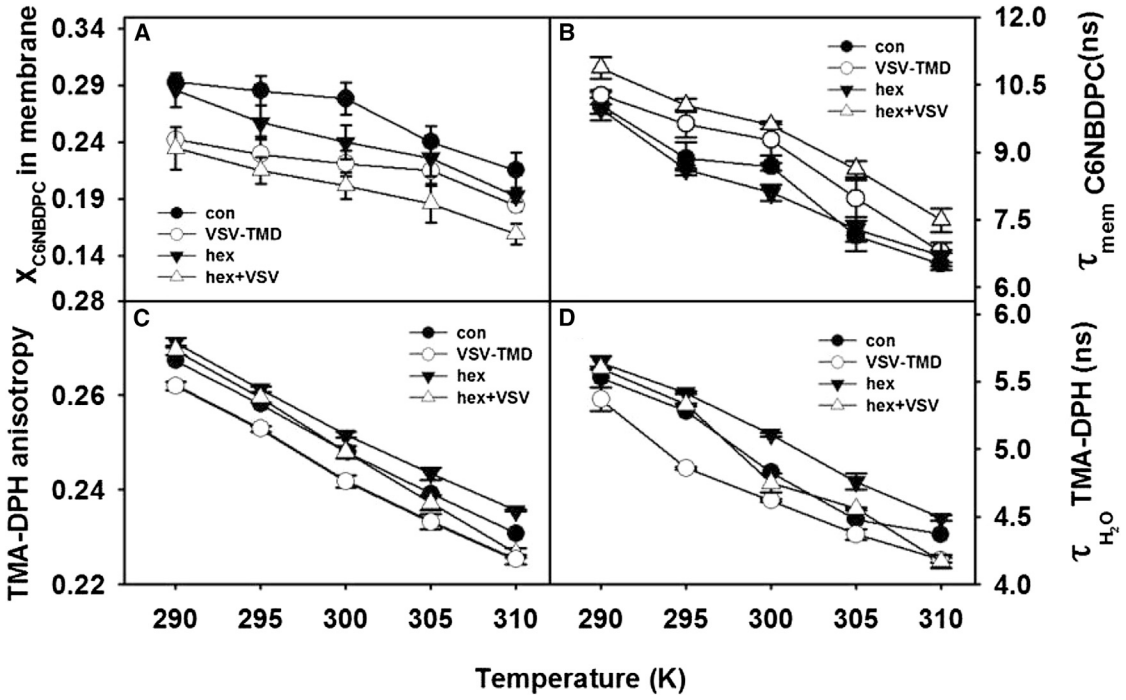

FIGURE 4 Effect of VSV-TMD, hexadecane, and hexadecane + TMD on the temperature dependence of (*A*) the mol fraction of C_6NBDPC in membranes, (*B*) the lifetime of C_6NBDPC in membranes, (*C*) TMA-DPH anisotropy, and (*D*) the fluorescence lifetime of TMA-DPH in membranes. Control SUVs (●) are compared with membranes containing hexadecane (▼), TMD peptide (○), and both hexadecane and TMD (Δ).

an event that is also consistent with the observed $T\Delta\Delta S_1^* > \Delta\Delta H_1^* > 0$ and increasingly negative $\Delta\Delta Cp_1^*$ with increasing temperature.

We note that VSV-TMD's catalytic influence on step 1 is entropic at all temperatures at pH 7.4 (Fig. 2 *B*), whereas that of hexadecane is entropic only at moderate temperatures and is enthalpic or inhibitory at high temperatures (18). This difference suggests that hexadecane and VSV-TMD have different mechanisms of action. Support for this proposal derives from the different mutual and individual effects of hexadecane and VSV-TMD on ΔG_1^* as plotted in Fig. 3 *A* as a function of temperature. Based on our membrane-structure measurements, VSV-TMD and hexadecane appear to alter bilayer structure in opposite ways at higher temperatures, with hexadecane reducing positive curvature stress and VSV-TMD increasing it (Fig. 4). At low temperature, where hexadecane has little influence on bilayer structure, it does not influence catalysis by VSV-TMD (Fig. 3 *A*). However, as temperature increases, the catalytic influence of hexadecane actually reduces the catalytic influence of VSV-TMD (Fig. 3 *A*). We propose that VSV-TMD catalyzes step 1 by increasing positive curvature stress in SUV outer leaflets in state A, whereas hexadecane decreases the outer-leaflet curvature stress of SUVs but catalyzes step 1 by promoting hydrocarbon-water contact in the TS1 intermediate (18). This hypothesis offers an explanation for the competing effects of VSV-TMD and hexadecane on step 1 (Fig. 3 *A*).

Step 3: conversion of intermediate to an FP state

The second semistable intermediate of the fusion process (I_2 in Fig. S3), which is detected at pH 5, is not detected at pH 7.4 because the free energy of the I_2 intermediate should increase at pH 7.4 due to reduced SUV outer-leaflet positive curvature stress at this pH (17,18). Thus, we propose that pores form at pH 7.4 by expansion of a stalk intermediate (I_1, stalk radius $= r_S \gtrsim 0$) via an unstable second intermediate (I_2) with an expanded *trans*-membrane contact (ETMC) geometry to an ETMC geometry with a critical stalk radius (r_S^*) at which transient pore expansion is more likely than pore reversal (see Fig. S3 for a detailed discussion of this proposal). The presence of VSV-TMD did not cause a reappearance of the second intermediate, so fusion at pH 7.4 is discussed in terms of a two-step process in the presence or absence of VSV-TMD (Tables 1 and S1).

We previously suggested that VSV-TMD might catalyze pore formation by occupying hydrophobic space and lowering the energy associated with the mismatch between lamellar and nonlamellar geometries (13) (interstice energy (17)). Hexadecane is known to lower this energy (36). At the lowest temperatures, hexadecane apparently aligns with acyl chains in hemifused *cis* leaflets, thereby contributing a positive intrinsic curvature that further destabilizes the ETMC circumference (18,27). However, with increasing temperatures, hexadecane apparently catalyzes pore formation by lowering interstice energy and promoting expansion

of ETMC microstructures at both pH 5 (19) and 7.4. At pH 7.4, $\Delta\Delta H_3^*$ for hexadecane varies from negative at the lowest temperatures to positive at intermediate temperatures and negative at the highest temperatures (18). If the catalytic influence of VSV-TMD on step 3 at pH 7.4 reflects its ability to fill interstice space and increase r_S toward r_S^*, the activation thermodynamics and catalytic influence of hexadecane and VSV-TMD should be similar, especially at higher temperatures. However, these were similar only at lower temperatures. In this temperature range (290–300 K), $\Delta\Delta H_3^*$ for VSV-TMDs was more than twice as negative as that for hexadecane (compare Fig. 2 *B* with Fig. 4 *F* of our companion article (18)). In addition, VSV-TMD's influence was clearly enthalpic at all temperatures, whereas that of hexadecane at pH 7.4 was less enthalpic and varied from enthalpic to entropic and then to enthalpic with increasing temperature (18). The simplest interpretation is that hexadecane and VSV-TMD catalyze pore formation by somewhat different mechanisms. The variation of hexadecane's catalytic influence with temperature likely reflects the variation of its conformational ensemble with temperature, i.e., being more aligned with acyl chains at lower temperatures, but being disordered and occupying hydrophobic interior space within the membrane at high temperatures (18,19,27). This suggests a possible interpretation of the observation that the catalytic effects of VSV-TMD and hexadecane were not additive at lower temperatures (Fig. 3 *B*). Thus, it may be that hexadecane and VSV-TMD catalyze pore formation by similar mechanisms at low temperature (i.e., they align with acyl chains and increase curvature stress at the ETMC circumference), but the influence of VSV-TMD is much greater than that of hexadecane, so that when both are present, the influence of VSV-TMD dominates. At higher temperatures, the catalytic influences of VSV-TMD and hexadecane were again both enthalpic. We interpret the enthalpic influence of VSV-TMD at this temperature as still reflecting its ability to increase curvature stress in hemifused *cis* leaflets at the ETMC circumference. On the other hand, it is likely that the influence of hexadecane in this temperature range is to increase the ETMC circumference by increasing the stalk radius (18,27). We conclude that VSV-TMD and hexadecane catalyze fusion by different mechanisms, except at lower temperatures, where the ability of VSV-TMD to increase curvature stress at the ETMC circumference is much greater than that of hexadecane.

We tested these interpretations by considering the effects of hexadecane and VSV-TMD on the total extent of CM (f_{CM}) and the probability of CM in the intermediate (α). Hexadecane increased the total extent of CM (f_{CM}), whereas VSV-TMD did not (Tables 1 and S1). In addition, whereas both hexadecane and VSV-TMD increased the probability of CM in the intermediate (α), hexadecane was more effective in this regard (Tables 1 and S1). We note that the total amount or extent of CM that occurs in the FP state $[(1-\alpha)\times f_{CM}]$ was the same for both perturbants (~0.15; Table 1). According to our hypothesis for VSV-TMD action, it achieves catalysis not by reducing interstice energy but by increasing positive curvature stress at a fixed ETMC diameter (r_S), i.e., by increasing the probability of CM earlier in the fusion process (i.e., it should increase α but not f_{CM}, as observed). By contrast, hexadecane promotes fusion by increasing the radius of the ETMC intermediate, which increases the number of fluctuations that can lead to transient pores before final pore formation (i.e., increasing α and f_{CM}). These observations support our hypothesis regarding the fundamentally different ways in which hexadecane and VSV-TMD catalyze fusion: VSV-TMD destabilizes the ETMC intermediate periphery at smaller stalk radii (i.e., it moves r_S^* to smaller r_S), and hexadecane promotes expansion of the ETMC intermediate to a point where it has a much larger periphery and thus an increased number of fluctuations that can form pores (i.e., it expands r_S toward r_S^*).

CONCLUSIONS

The data and analysis presented here for PEG-mediated fusion of DOPC/DOPE/SM/CH SUVs at pH 7.4 are all consistent with the hypothesis that VSV-TMD catalyzes step 1 of the fusion process by occupying the upper bilayer space to facilitate acyl-chain excursions into the interbilayer space, thereby promoting the conversion of closely opposed monolayers to stalk intermediate microstructures, and catalyzes step 3 of the fusion process by occupying the upper bilayer space so as to increase curvature stress at the periphery of expanded intermediate microstructures. We previously proposed that this stress promotes correlated lipid fluctuations into interstice regions to produce transiently stable pores (19). In addition, we have shown that VSV-TMD promotes stable pore formation by a mechanism quite different from that proposed for hexadecane (18).

Finally, although hexadecane and VSV-TMD share similar activation thermodynamics for initial intermediate formation at low temperature, it appears that they do not share a common mechanism for catalyzing this step of fusion at any temperature, with VSV-TMD enthalpically destabilizing the contacting bilayers of the A state, and hexadecane entropically stabilizing the water-hydrocarbon environment of the TS1 state (18). This is in contrast to the previous suggestion that VSV-TMD might act by filling the interstice space, as does hexadecane at higher temperatures (13).

SUPPORTING MATERIAL

Three figures, two tables, and Supporting References are available at http://www.biophysj.org/biophysj/supplemental/S0006-3495(14)00794-2.

We thank Dr. Pradip Tarafdar for many useful discussions and especially acknowledge the efforts of two reviewers whose careful and substantial comments allowed us to greatly improve the presentation of our results and conclusions.

This work was supported by U.S. Public Health Service grant GM32707 to B.R.L.

REFERENCES

1. Bullough, P. A., F. M. Hughson, …, D. C. Wiley. 1994. Structure of influenza haemagglutinin at the pH of membrane fusion. *Nature.* 371:37–43.
2. Yin, H. S., R. G. Paterson, …, T. S. Jardetzky. 2005. Structure of the uncleaved ectodomain of the paramyxovirus (hPIV3) fusion protein. *Proc. Natl. Acad. Sci. USA.* 102:9288–9293.
3. Harrison, S. C. 2008. Viral membrane fusion. *Nat. Struct. Mol. Biol.* 15:690–698.
4. White, J. M., S. E. Delos, …, K. Schornberg. 2008. Structures and mechanisms of viral membrane fusion proteins: multiple variations on a common theme. *Crit. Rev. Biochem. Mol. Biol.* 43:189–219.
5. Burgess, S. W., T. J. McIntosh, and B. R. Lentz. 1992. Modulation of poly(ethylene glycol)-induced fusion by membrane hydration: importance of interbilayer separation. *Biochemistry.* 31:2653–2661.
6. Kemble, G. W., T. Danieli, and J. M. White. 1994. Lipid-anchored influenza hemagglutinin promotes hemifusion, not complete fusion. *Cell.* 76:383–391.
7. Nüssler, F., M. J. Clague, and A. Herrmann. 1997. Meta-stability of the hemifusion intermediate induced by glycosylphosphatidylinositol-anchored influenza hemagglutinin. *Biophys. J.* 73:2280–2291.
8. Odell, D., E. Wanas, …, H. P. Ghosh. 1997. Influence of membrane anchoring and cytoplasmic domains on the fusogenic activity of vesicular stomatitis virus glycoprotein G. *J. Virol.* 71:7996–8000.
9. Miyauchi, K., R. Curran, …, Z. Matsuda. 2006. Mutations of conserved glycine residues within the membrane-spanning domain of human immunodeficiency virus type 1 gp41 can inhibit membrane fusion and incorporation of Env onto virions. *Jpn. J. Infect. Dis.* 59:77–84.
10. Owens, R. J., C. Burke, and J. K. Rose. 1994. Mutations in the membrane-spanning domain of the human immunodeficiency virus envelope glycoprotein that affect fusion activity. *J. Virol.* 68:570–574.
11. Shang, L., L. Yue, and E. Hunter. 2008. Role of the membrane-spanning domain of human immunodeficiency virus type 1 envelope glycoprotein in cell-cell fusion and virus infection. *J. Virol.* 82:5417–5428.
12. Cleverley, D. Z., and J. Lenard. 1998. The transmembrane domain in viral fusion: essential role for a conserved glycine residue in vesicular stomatitis virus G protein. *Proc. Natl. Acad. Sci. USA.* 95:3425–3430.
13. Dennison, S. M., N. Greenfield, …, B. R. Lentz. 2002. VSV transmembrane domain (TMD) peptide promotes PEG-mediated fusion of liposomes in a conformationally sensitive fashion. *Biochemistry.* 41: 14925–14934.
14. Melikyan, G. B., R. M. Markosyan, …, F. S. Cohen. 2000. A point mutation in the transmembrane domain of the hemagglutinin of influenza virus stabilizes a hemifusion intermediate that can transit to fusion. *Mol. Biol. Cell.* 11:3765–3775.
15. Cohen, F. S., and G. B. Melikyan. 2004. The energetics of membrane fusion from binding, through hemifusion, pore formation, and pore enlargement. *J. Membr. Biol.* 199:1–14.
16. Chernomordik, L. V., and M. M. Kozlov. 2003. Protein-lipid interplay in fusion and fission of biological membranes. *Annu. Rev. Biochem.* 72:175–207.
17. Malinin, V. S., and B. R. Lentz. 2004. Energetics of vesicle fusion intermediates: comparison of calculations with observed effects of osmotic and curvature stresses. *Biophys. J.* 86:2951–2964.
18. Chakraborty, H., T. Sengupta, and B. R. Lentz. 2014. pH alters PEG-mediated fusion of phosphatidylethanolamine-containing vesicles. *Biophys. J.*: In review.
19. Chakraborty, H., P. K. Tarafdar, …, B. R. Lentz. 2012. Activation thermodynamics of poly(ethylene glycol)-mediated model membrane fusion support mechanistic models of stalk and pore formation. *Biophys. J.* 102:2751–2760.
20. Le Blanc, I., P. P. Luyet, …, J. Gruenberg. 2005. Endosome-to-cytosol transport of viral nucleocapsids. *Nat. Cell Biol.* 7:653–664.
21. Roche, S., F. A. Rey, …, S. Bressanelli. 2007. Structure of the prefusion form of the vesicular stomatitis virus glycoprotein G. *Science.* 315:843–848.
22. Weinreb, G., and B. R. Lentz. 2007. Analysis of membrane fusion as a two-state sequential process: evaluation of the stalk model. *Biophys. J.* 92:4012–4029.
23. Lee, J., and B. R. Lentz. 1997. Evolution of lipidic structures during model membrane fusion and the relation of this process to cell membrane fusion. *Biochemistry.* 36:6251–6259.
24. Chen, P. S., T. Y. Toribara, and H. Warner. 1956. Microdetermination of phosphate. *Anal. Chem.* 28:1756–1758.
25. Schwenk, E., and N. T. Werthessen. 1952. Studies on the biosynthesis of cholesterol. III. Purification of C14-cholesterol from perfusions of livers and other organs. *Arch. Biochem. Biophys.* 40:334–341.
26. Lentz, B. R., G. F. McIntyre, …, D. Massenburg. 1992. Bilayer curvature and certain amphipaths promote poly(ethylene glycol)-induced fusion of dipalmitoylphosphatidylcholine unilamellar vesicles. *Biochemistry.* 31:2643–2653.
27. Chakraborty, H., P. K. Tarafdar, …, B. R. Lentz. 2013. Wild-type and mutant hemagglutinin fusion peptides alter bilayer structure as well as kinetics and activation thermodynamics of stalk and pore formation differently: mechanistic implications. *Biophys. J.* 105:2495–2506.
28. Kyoung, M., A. Srivastava, …, A. T. Brunger. 2011. In vitro system capable of differentiating fast Ca2+-triggered content mixing from lipid exchange for mechanistic studies of neurotransmitter release. *Proc. Natl. Acad. Sci. USA.* 108:E304–E313.
29. Lee, J., and B. R. Lentz. 1997. Outer leaflet-packing defects promote poly(ethylene glycol)-mediated fusion of large unilamellar vesicles. *Biochemistry.* 36:421–431.
30. Ho, C., S. J. Slater, and C. D. Stubbs. 1995. Hydration and order in lipid bilayers. *Biochemistry.* 34:6188–6195.
31. Tarafdar, P. K., H. Chakraborty, …, B. R. Lentz. 2012. Phosphatidylserine inhibits and calcium promotes model membrane fusion. *Biophys. J.* 103:1880–1889.
32. Haque, M. E., H. Chakraborty, …, B. R. Lentz. 2011. Hemagglutinin fusion peptide mutants in model membranes: structural properties, membrane physical properties, and PEG-mediated fusion. *Biophys. J.* 101:1095–1104.
33. Siegel, D. P. 1999. The modified stalk mechanism of lamellar/inverted phase transitions and its implications for membrane fusion. *Biophys. J.* 76:291–313.
34. Smirnova, Y. G., S. J. Marrink, …, V. Knecht. 2010. Solvent-exposed tails as prestalk transition states for membrane fusion at low hydration. *J. Am. Chem. Soc.* 132:6710–6718.
35. Kasson, P. M., E. Lindahl, and V. S. Pande. 2010. Atomic-resolution simulations predict a transition state for vesicle fusion defined by contact of a few lipid tails. *PLOS Comput. Biol.* 6:e1000829.
36. Kozlov, M. M., S. Leikin, and R. P. Rand. 1994. Bending, hydration and interstitial energies quantitatively account for the hexagonal-lamellar-hexagonal reentrant phase transition in dioleoylphosphatidylethanolamine. *Biophys. J.* 67:1603–1611.

Supplemental Material for

The Transmembrane Domain Peptide of Vesicular Stomatitis Virus Promotes Both Intermediate and Pore Formation during PEG-mediated Vesicle Fusion.

Tanusree Sengupta[†], Hirak Chakraborty[†], Barry R. Lentz[*]

Department of Biochemistry and Biophysics & Program in Molecular and Cellular Biophysics

University of North Carolina at Chapel Hill, North Carolina 27599-7260

[†] Authors contributed equally

[*]Correspondence: Barry R. Lentz, Department of Biochemistry and Biophysics & Program in Molecular and Cellular Biophysics, University of North Carolina at Chapel Hill, NC 27599. Phone: 919-966-5384. Email: uncbrl@med.unc.edu

Present Address of Hirak Chakraborty: Centre for Cellular and Molecular Biology, Council of Scientific and Industrial Research, Hyderabad 500 007, India.

Present Address of Tanusree Sengupta: Department of Biotechnology, Indian Institute of Technology Madras, Chennai 600 036, India

Samples	$k_1 \times 10^3$ (sec^{-1})	$k_3 \times 10^3$ (sec^{-1})	α	β	$\lambda_0 \times 10^4$	$\lambda_2 \times 10^4$	$\lambda_3 \times 10^4$	f_{CM}	f_{LM}
17°C_con	10.0± 0.5	1.08± 0.05	0.16± 0.01	0.49± 0.01	2.67 ±0.04	2.06± 0.02	0.52±0.06	0.15± 0.01	0.38± 0.01
17°C_vsv	19.3± 0.6	2.27± 0.02	0.41± 0.01	0.58± 0.01	5.49 ± .08	3.06± 0.03	0.57±0.15	0.24± 0.01	0.43± 0.01
17°C_hex	11.1± 0.6	1.54± 0.04	0.57± 0.01	0.41± 0.01	3.25 ±0.11	2.51± 0.05	0.21 ±0.22	0.35± 0.01	0.40± 0.01
17°C_hex+ vsv	22.0± 0.6	2.65± 0.04	0.58± 0.01	0.60± 0.01	11.36±0.23	3.85± 0.07	0.42±0.17	0.33± 0.02	0.39± 0.01
27°C_con	21.5± 0.9	2.22 ± 0.02	0.25± 0.01	0.62± 0.01	3.81± 0.10	3.00± 0.05	0.77±0.23	0.26± 0.01	0.46± 0.02
27°C_VSV	40.0 ± 1.0	3.06 ± 0.04	0.49± 0.01	0.69± 0.01	11.82±0.36	5.45± 0.03	0.74± 0.15	0.28± 0.01	0.47± 0.02
27°C_hex	27.5± 1.2	2.63± 0.03	0.70± 0.03	0.72± 0.03	15.86±0.27	5.37± 0.07	5.01±0.21	0.41± 0.02	0.44± 0.03
27°C_hex+ vsv	37.2 ± 1.1	2.96 ± 0.05	0.63 ± 0.02	0.62± 0.02	29.55±0.36	5.75± 0.09	5.57±0.23	0.39± 0.03	0.42± 0.01
32°C_con	33.1± 0.7	2.65 ±0.05	0.32± 0.01	0.72± 0.01	9.42± 0.31	4.69± 0.07	0.79± 0.25	0.36± 0.01	0.45± 0.01
32°C_VSV	75.0 ± 1.0	3.28 ±0.04	0.51± 0.01	0.75± 0.01	27.37±0.32	7.10 ± 0.04	9.26 ±0.23	0.35± 0.02	0.45± 0.01
32°C_hex	48.5± 1.2	3.57± 0.06	0.64± 0.02	0.75± 0.02	36.44±0.55	7.55± 0.13	3.45 ±0.23	0.41± 0.02	0.44± 0.01
32°C_hex+ VSV	57.9 ± 1.1	3.34± 0.07	0.64± 0.01	0.74± 0.01	51.94±0.04	6.81± 0.09	7.54±0.51	0.40 ±0.01	0.44± 0.03

Table S1. Different kinetic parameters of the fusion reaction in PC/PE/SM/CH (35/30/15/20) membrane system in presence of 2% hexadecane, VSV-TMD and hexadecane + VSV-TMD at different temperatures.

		y_0	a_i	b_i	c_i
Control	First Step	4762.4 ± 651.7	-47.90 ± 6.52	0.16 ± 0.022	$-2x10^{-4}$ ± 2.42×10^{-5}
Control	Second Step	1412.6 ± 89.86	-13.72 ± 0.89	0.045 ± 0.003	-4.83×10^{-5} ± 3.33×10^{-6}
VSV-TMD	First Step	-3090.89 ± 200.63	30.74 ± 10.07	-0.10 ± 0.04	$1x10^{-4}$ ± 7.43×10^{-5}
VSV-TMD	Second Step	-1771.52 ± 142.33	17.89 ± 4.28	-0.06 ± 0.01	6.72×10^{-5} ± 1.29×10^{-5}

Table S2. Parameters obtained by fitting the plot of ΔG_i^* vs. temperature (Figure 2) using the equation $\Delta G_i^*(kcal/mol) = y_{0,i} + a_i T + b_i T^2 + c_i T^3$ for the fusion of control vesicles and vesicles prepared in presence of VSV-TMD (Figure 4). The same parameters were used to obtain $T\Delta S_i^*$ ($-a_i T - 2b_i T^2 - 3c_i T^3$); ΔH_i^* ($y_{0,i} - b_i T^2 - 2c_i T^3$), and ΔCp_i^* ($-2b_i T - 6c_i T^2$).

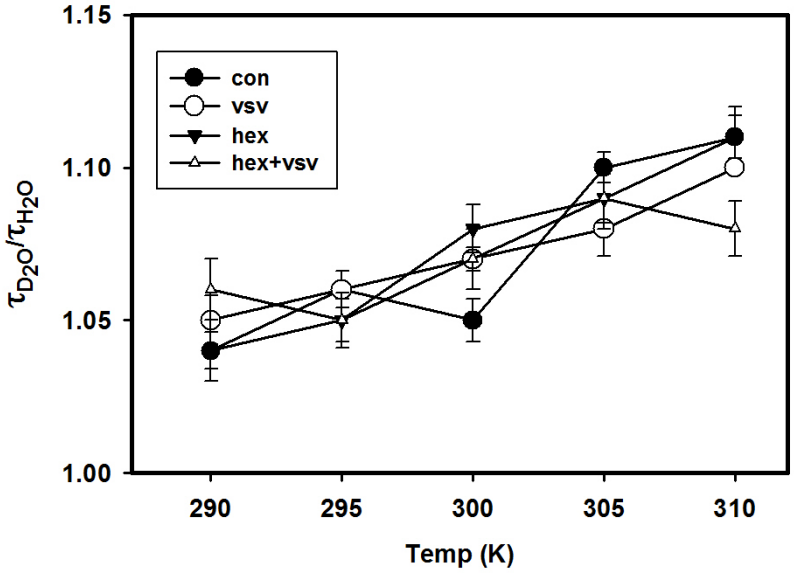

Figure S1. Plot of ratio of lifetime of TMA-DPH in membrane made in D_2O and H_2O buffer in control membrane (●) and membrane containing VSV-TMD (○) (L/P=600/1), 2% hexadecane (▼) and both hexadecane and VSV TMD (Δ) at five different temperature.

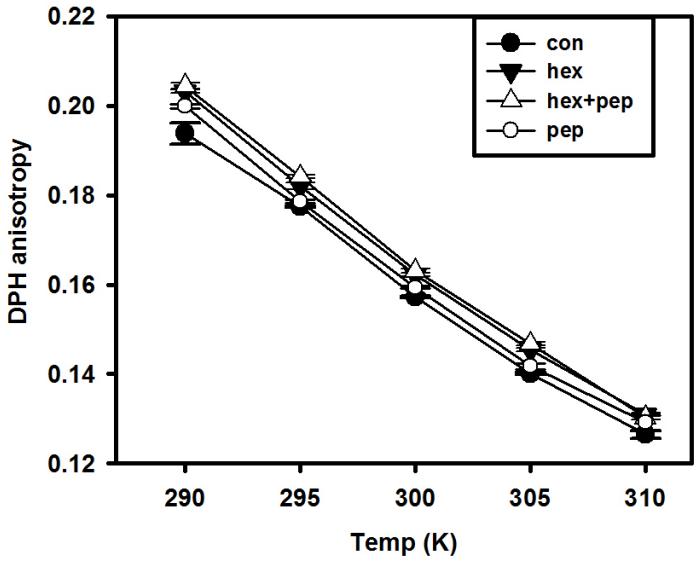

Figure S2. Effect of TMD, hexadecane, and hexadecane + TMD on acyl chain packing of membranes. DPH fluorescence emission anisotropy of control vesicles (●) and vesicles containing VSV (○), hexadecane (▼) and both hexadecane and VSV (Δ) different species are shown at different five temperatures (lipid: probe = 200:1).

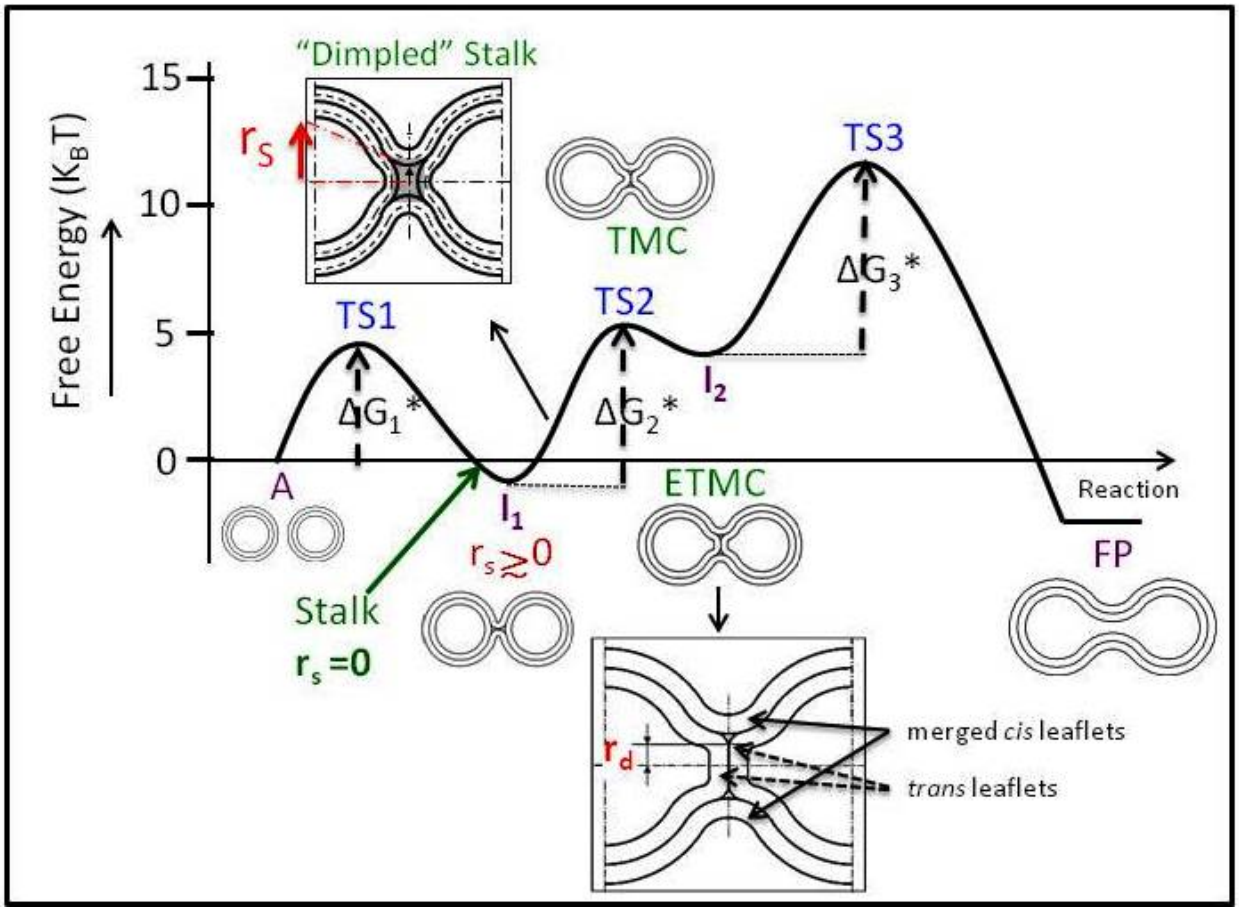

Figure S3. Our kinetic model (see Diagram) derives from the expanded-stalk structural model of Siegel for lamellar to non-lamellar phase transitions as applied to membrane fusion. We adapted this model in order to calculate the activation free energy path for the transition of an initial hemi-fused state (I_1, initial intermediate) between two highly stressed SUVs to a second semi-stable state (I_2) from which a fusion pore state (FP) can form. Two free energy minima confirmed the two-step nature of the fusion path as depicted in our model and as detected experimentally. The geometries (labeled in green) of the predicted intermediates are shown for intermediate structures derived from minimization of the free energies of structures at fixed stalk radii (1). Unstable "transition states" are labeled in blue and semi-stable intermediate "states" in purple. The "reaction coordinate" for this diagram is the "stalk radius" (r_s) that is illustrated in the "dimpled stalk" diagram and is defined as "0" when the two merged *cis*- leaflets first touch. Since our experiments are performed on vesicle ensembles, each "state" is a thermodynamic state and does not correspond to a single structure. In the context of the large-scale mechanical computation, the first state encountered as r_s increases is I_1, which is commonly called the stalk, but occurs at a slightly larger stalk radius than the stalk. The driving force for evolution of the system along its reaction coordinate is a reduction in positive curvature stress that overcomes an increase in unfavorable interstice energy as r_s increases. "Interstices" are regions at the edge of the hemi-fused region (shaded regions in figure) for which lamellar and non-lamellar lipid packing conflict. Because water-hydrocarbon interactions are required to compensate for this mismatch, this leads to an unfavorable "interstice" free

energy. The evolution from I_1 to I_2 proceeds through a *trans*-membrane contact (TMC) first described by Siegel that provides an unstable transition state to reaching the I_2 semi-stable intermediate, which corresponds to a slight minimum in free energy in a geometry described by Siegel as an "extended *trans*-membrane contact" (ETMC). The depth of the I_1 and I_2 free energy minima as well as the height of the TS2 barrier are all subject to variation with the particular natures of different membrane systems (*e.g.*, composition, pH, vesicle diameter, *etc.*). Thus, the membrane system DOPC/DOPE/SM/CH that we examine here passes through two intermediates when fusing at pH 5 but only one at pH 7.4, as we report here. The TS2 transition state is the only one appropriately predicted by the materials-scale materials model. The first and third steps involve changes from 2-compartment, to hemi-fused, to single-compartment topologies that require molecular rearrangements that cannot be described in terms of materials-scale mechanical models. We have used measured activation thermodynamics for each step and measured membrane structural properties to suggest possible mechanistic models for these molecular rearrangements, and here ask whether these are consistent with observations made in the presence VSV-TMD. The ΔG_1^* and ΔG_3^* magnitudes shown are illustrative of but not exact matches to experimental values obtained for k_1 and k_3.

This figure has been adapted from the Supplemental Material of (2) with permission of the publisher (cell Press).

REFERENCES

1. Malinin, V. S., and B. R. Lentz. 2004. Energetics of vesicle fusion intermediates: comparison of calculations with observed effects of osmotic and curvature stresses. *Biophys. J.* 86:2951-2964.

2. Chakraborty, H., P. K. Tarafdar, M. J. Bruno, T. Sengupta, and B. R. Lentz. 2012. Activation Thermodynamics of PEG-Mediated Model Membrane Fusion Are Consistent with Mechanistic Models of Stalk and Pore Formation. *Biophys. J.* 102:2751-2760.